Journal of Sound and Vibration 329 (2010) 3495–3506

Contents lists available at ScienceDirect

Journal of Sound and Vibration

journal homepage: www.elsevier.com/locate/jsvi

An investigation into the effect of tooth profile errors on gear rattle

J.R. Ottewill [a,*], S.A. Neild [a,**], R.E. Wilson [b]

[a] Department of Mechanical Engineering, University of Bristol, Bristol BS8 1TR, UK
[b] Bristol Centre for Applied Nonlinear Mathematics, University of Bristol, Bristol BS8 1TR, UK

ARTICLE INFO

Article history:
Received 18 October 2009
Received in revised form
8 March 2010
Accepted 9 March 2010
Handling Editor: L.N. Virgin
Available online 9 April 2010

ABSTRACT

In previous work, experimental data have demonstrated the severity of idling gear rattle depends not only on the amplitude, but also the phase of an external sinusoidal forcing. One possible explanation for this is in small tooth profile errors. In this paper, we investigate this hypothesis, by deriving an equation of motion incorporating an error function and losses at the mesh interface, values of which are obtained from experimental data. By solving the equations of motion, theoretical gear rattle trajectories are obtained. Theoretical and experimental trajectories are then compared, by way of time domain plots as well as via contour plots linking the amplitude of backlash oscillation to the amplitude and phase of input forcing. For most profile error functions, good agreement is achieved between the model and experimental data. In the case where the profile errors are dominated by misalignment between the gear and shaft centres agreement is less good and suggestions of areas of further study required for model refinement are proposed.

1. Introduction

In attempting to increase the efficiency of their rotating machinery (e.g. by decreasing the viscosity of lubricants) manufacturers have begun to observe undesirable vibrations in their components which were previously suppressed or masked. The rattle of gears as they oscillate within their backlash is an example of a dynamic phenomenon that has recently received increased attention for this reason. Although the problem of gear rattle is not isolated to the automotive gearbox, it is widely recognised as a noise, vibration and harshness (NVH) problem, occurring in the lightly loaded, unselected gear pairs of a transmission [1,2]. These gear pairs are subject to a vibratory excitation due to the firing sequence of the engine. As the gears are effectively unloaded, tooth profile errors, a known source of excitation for gear noise [3], are also likely to play an important role. In this paper we consider the interaction between the external input excitation and the internal excitation due to tooth profile errors.

Since the first spring-mass vibratory models of Tuplin [4], many efforts have been made to incorporate the effect of tooth profile manufacturing errors into gear dynamics models [5]. As a mechanism relying on the sliding and rolling of teeth of non-trivial geometries, gears are particularly susceptible to the manufacturing errors that inevitably occur. First described by Harris [6], the static transmission error (STE) is a function that describes how the angular position of a driven gear deviates from perfect conjugate motion. The STE is regularly incorporated into equations of motion for gear pairs as a

* Principal corresponding author.
** Corresponding author. Tel.: +44 1173315918.
E-mail addresses: jamesottewill@hotmail.co.uk (J.R. Ottewill), Simon.Neild@bristol.ac.uk (S.A. Neild).

0022-460X/$ - see front matter © 2010 Elsevier Ltd. All rights reserved.
doi:10.1016/j.jsv.2010.03.014

Nomenclature

a_j	amplitude of component with frequency j
b	mesh interaction force
c	viscous linear coefficient
d	phase of STE component due to eccentricity (see Ref. [14])
e	no-load static transmission error
f	set of frequencies comprising the recreated STE function
I	moment of inertia
r_b	base circle radius
t	time
U	amplitude of STE component due to eccentricity (see Ref. [14])
x	dynamic transmission error
β	half backlash size (rad)
δ	non-dimensional damping coefficient
ε	non-dimensionalised torque oscillation amplitude
ς	coefficient of restitution
θ	rotational displacement (rad)
τ	non-dimensionalised time
$\tau_{\text{impact}+(-)}$	non-dimensionalised time an instant before (after) impact
ϕ	phase of forcing input
ϕ_j	phase of component with frequency j
Ψ	initial angle of the driven gear relative to the drive gear
Ω	gross rotation rate (Hz)

Subscripts

$()_\infty$	value as time tends to infinity
$()_1$	denotes driving gear
$()_2$	denotes driven gear
$()_{\text{pos}}$	denotes values occurring on the 'positive' drive surface
$()_{\text{neg}}$	denotes values occurring on the 'negative' drive surface
$()_{\text{contact}}$	value occurring when gears are meshing ('in contact')

Superscripts

$\dot{()}$	first derivative with respect to time (velocity)
$\ddot{()}$	second derivative with respect to time (acceleration)
$()'$	first derivative with respect to non-dimensionalised time
$()''$	second derivative with respect to non-dimensionalised time

displacement-type excitation occurring at the interface [7–11]. The form which this function takes is dictated by the stiffness and geometries of the meshing gear pair.

When considering lightly loaded gear rattle, many studies have considered the primary excitation source to be an external, low frequency oscillatory forcing. This is driven by the fact that in practice, gear rattle occurs at frequencies closely matched to the harmonics of engine speed [12]. It has been shown by a number of authors that gear rattle will occur when the inertial torque of the unloaded, 'loose' gear overcomes the drag torques, for example [1,13]. In a recent paper [14], the authors investigated this rattle threshold experimentally, finding that the phase of the input vibratory excitation, relative to the angular position of the gear pairs, can have a significant effect on the magnitude of rattle response. It was suggested that tooth profile errors may be the cause of these variations in rattle amplitude.

In this paper we show evidence that the STE has a major effect on loose gear rattle. We accomplish this by linking our experimental findings given in [14] with results predicted by a low-degree-of-freedom lumped parameter model for idling gear rattle. The aim of the proposed model is to capture the dynamics of the gear pair as accurately as possible, using relatively few physical design parameters, with the aim of developing expressions linking these key parameters to the response of the system. By using an averaging and selective filtering process, we synthesise a STE function from the experimental data, which we then substitute into our model as a displacement excitation at the interface. Furthermore, friction between the meshing teeth is inevitable and has been suggested to play a considerable role in gear dynamics [15–19]. Thus we incorporate a meshing damping term, describing the frictional losses incurred as the gear teeth rub against one another. The approximate value of this parameter is obtained experimentally via a run-down test. Using a combination of numerical and analytical methods we calculate trajectories of relative gear motion which we are able to compare directly with experimental findings. We draw conclusions as to the effect of STE on gear rattle from cases where we obtain good agreement and offer suggestions for future work to enhance the accuracy of the model.

2. Experimental rig

The experimental rig, shown in Fig. 1 (and described in detail in [14]) consisted of gear pair, with each gear attached to a high accuracy optical encoder. A servomotor was used to drive one of the gears (the *drive* gear). The second gear was unloaded and represents the idling or *driven* gear. Since the idling gear is unloaded it is assumed that it does not affect the motion of the driven gear, hence the servomotor was controlled in angular displacement (using a proportional plus derivative feedback controller). The 1:1 ratio gears employed were of high module and the shaft diameters were large, allowing the system to be considered rigid. Although 1:1 ratio gear pairs are seen in some industries (for example in roots booster pumps, a device in which rattle has been reported [20]), many other gear systems, including the automotive case motivating this research, utilise gears of differing size. However, by considering 1:1 ratio gears multiple STEs were able to

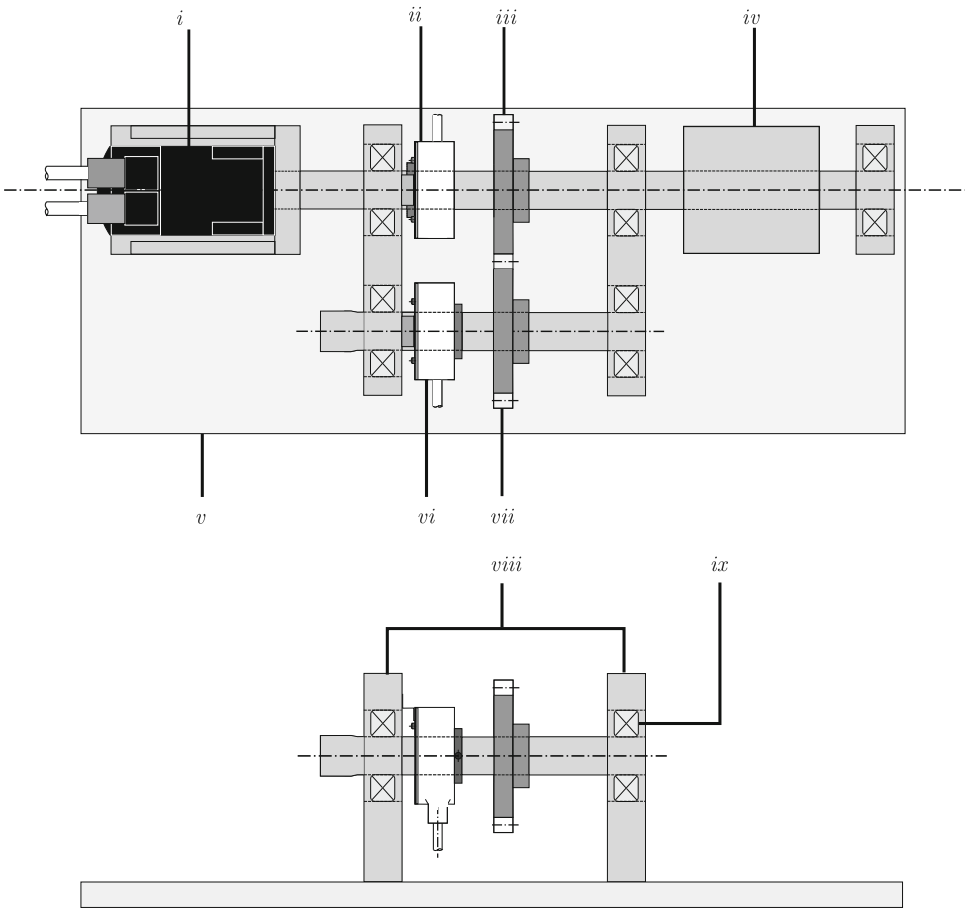

Fig. 1. Experimental rig. (i) Electronic brushless servo motor; (ii) drive side encoder, both encoders are Hengstler RI76-TD Series hollow shaft incremental encoders, with 10,000 pulses per revolution (giving a resolution of 1.57×10^{-4} rad by detecting each pulse edge); (iii) drive gear, both gears are module 6, 108 mm pitch circle diameter, mild steel spur gears precision ground to BS436 Grade 6 (equivalent to ISO 1328-2) standard; (iv) inertial mass; (v) base plate, bolted to a table of large mass to eliminate the possibility of any undesirable vibrational modes; (vi) driven side encoder; (vii) driven gear; (viii) bearing housings; (ix) single row radial ball bearings, shaft diameter is 30 mm.

be investigated without drastically altering the experimental set-up. Furthermore, the findings of [14] are relevant to non-unity gear pairs; the STE simply has a larger periodicity. By applying a sinusoidally varying displacement input, centred about a constant rate of rotation as an input to the experimental system, we were able to conduct experiments analogous to the lightly loaded rattle observed in automotive transmissions. This resulted in a drive gear angular displacement demand, θ_1, given by

$$\theta_1 = 2\pi\Omega t + \varepsilon\cos(2\pi\Omega t + \phi), \tag{1}$$

where Ω is the gross rotation rate of the gears, ε is the amplitude of the sinusoidal forcing and ϕ is the phase of the forcing (which is set relative to the initial orientation of the gears).

In [14] it was observed that at the same amplitude of displacement excitation forcing, large variations in the magnitude of any contact losses between the gears (which we term 'disconnections' for brevity) were possible, the variations being dependent on the phase of the displacement excitation relative to the angular positions of the gears. In a geared system with no profile errors, changing the phase of the input would have no effect. However, in a real system, the inevitable profile errors meant that the total forcing transmitted between the gears would be a superposition of the external displacement excitation and the internal forcing due to the STE. Changing the phase of the input changed the magnitude of this superposition.

3. Mathematical model

Fig. 2 shows a schematic diagram of the gear pair model, an impacting model in which it is assumed that there is no compliance as the driven gear is not loaded. Subscript 1 denotes the drive gear which moves with a defined displacement, and subscript 2 denotes the driven gear. By resolving the moments acting upon the driven gear the equation of motion is

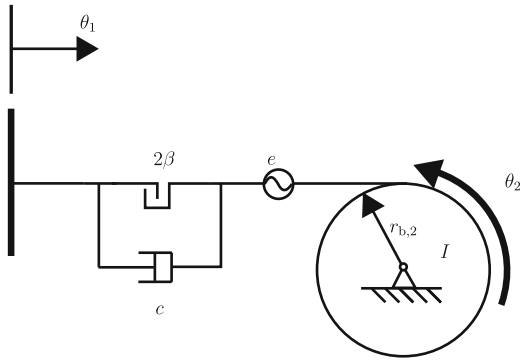

Fig. 2. A schematic of the simple model for gear rattle.

obtained

$$I\ddot{\theta}_2 + c\dot{\theta}_2 = b(\theta_1,\theta_2,2\beta,e_{\text{pos}},e_{\text{neg}}), \tag{2}$$

where I is the moment of inertia of the gear, c is the viscous linear friction coefficient, and θ is the angular displacement of each gear. The interaction force between the gears, b, is a function of the angular position of the gears, the size of the backlash clearance, 2β, and a no-load STE displacement function, e. Here e_{pos} represents errors on the 'positive' drive surface, where the drive gear is driving the driven gear (as generally is intended), whilst e_{neg} indicates where the opposite is true and torque transfer is reversed. The no-load STE function is itself a function of the angular position and the individual tooth profile errors of each gear,

$$e_{\text{pos}}(\theta_1,\theta_2,e_{1,\text{pos}}(\theta_1),e_{2,\text{pos}}(\theta_2)), \tag{3}$$

$$e_{\text{neg}}(\theta_1,\theta_2,e_{1,\text{neg}}(\theta_1),e_{2,\text{neg}}(\theta_2)). \tag{4}$$

As we are primarily interested in calculating the point of transition from meshing on the positive drive surface to being out of contact, we make the simplifying assumption that we may neglect e_{neg}. We do this by setting $e_{\text{neg}}=e_{\text{pos}}=e$. The experimental results were obtained with 1:1 ratio gears, allowing us to simplify e to be a function of θ_1 and an initial relative orientation of the driven gear relative to the drive gear, Ψ. We obtain

$$e(\theta_1,\theta_2,e_1(\theta_1),e_2(\theta_2)) = e(\theta_1,\Psi,e_1(\theta_1),e_2(\theta_1+\Psi)). \tag{5}$$

The drive gear moves with prescribed angular displacement, θ_1 given by Eq. (1). Usually, the individual tooth profile errors e_1 and e_2 are unknown prior to installation of the gear pair. The STE is not deterministic; two gear pairs manufactured to identical tolerances are likely to have completely different STE functions. Furthermore, additional mounting errors and misalignments are likely to occur. It is therefore preferable to consider simply the no-load STE purely as an unknown function which is dependent on time, t. This function is periodic with each complete rotation of a gear.

We define a dynamic transmission error, x, which is normalised to the top backlash boundary, as

$$x = \theta_1 - \theta_2 - e(t). \tag{6}$$

The dynamic transmission error, x is centred in the middle of the backlash gap. Therefore, when $x=\beta$, the drive gear is driving the driven gear, whereas when $x=-\beta$ the driven gear is driving the drive gear. By substituting Eqs. (1), (6) into Eq. (2) we may obtain

$$x'' + \delta x' + b(x,2\beta) = \theta_1'' + \delta\theta_1' - e''(\tau) - \delta e'(\tau) = 2\pi\delta - 2\pi\varepsilon\sqrt{4\pi^2+\delta^2}\cos\left(2\pi\tau+\phi-\arctan\left(\frac{\delta}{2\pi}\right)\right) - e''(\tau) - \delta e'(\tau), \tag{7}$$

where $\{\}'$ is the derivative with respect to non-dimensional time ($\tau=\Omega t$) and non-dimensional damping, δ, is given by

$$\delta = \frac{c}{I\Omega}. \tag{8}$$

As the stiffness is high whilst the driven gear is unloaded, we may assume that there is minimal deformation at impact. When the gears are out of contact with one another, in free-play motion, the interaction force between the two gears, b, is zero. Hence,

$$x'' + \delta x' = 2\pi\delta - 2\pi\varepsilon\sqrt{4\pi^2+\delta^2}\cos\left(2\pi\tau+\phi-\arctan\left(\frac{\delta}{2\pi}\right)\right) - e''(\tau) - \delta e'(\tau) \quad \text{for } |x|<\beta. \tag{9}$$

When the two gears impact, at $|x|=\beta$, the integration constants of the solution to Eq. (9) must be re-evaluated with new initial conditions defined by the time and velocity of impact, $\tau=\tau_{\text{impact}}$. We assume impacts may be satisfactorily described

by a Newtonian coefficient of restitution based model,

$$x(\tau_{\text{impact}+}) = x(\tau_{\text{impact}-}),$$

$$x'(\tau_{\text{impact}+}) = -\varsigma x'(\tau_{\text{impact}-}), \tag{10}$$

where ς is the coefficient of restitution and subscripts $-$ and $+$ indicate an instant before and after impact, respectively. We therefore have an equation of motion where the free motion of the driven gear is dictated by the forcing due to the applied input from the driven gear and the forcing due to the interface errors between the drive and the driven gear. Note that by making the assumption that the system is rigid, we are also assuming the no-load STE is equal to a loaded STE. From now on we refer to the no-load STE as simply the STE.

4. Synthesis of an error function

STE functions were generated experimentally by running the gears at a constant low velocity ($\Omega = 1$ Hz,$\varepsilon = 0$). Assuming minimal deformation (as the driven gear was unloaded, the gear pair was of high module and the rig was run at a constant low speed) the STE of the gears was recorded as the relative angular displacement of the two encoders. Usually, the largest component will occur at the same frequency as gross rotation rate of the rig, being caused by eccentric mountings. Other profile errors are typically much smaller in amplitude. A recorded STE for one rotation is shown in Fig. 3(a). Due to the size of the errors being measured, the data are quantised; note that one quantum corresponds to 1.57×10^{-4} rad or an arc length of 8.5 μm at the pitch circle radius. A more accurate STE was recorded by splitting a 25 s long signal into 1 s intervals so that it corresponds to each complete rotation of the gears and taking the average relative displacement for each point in time. A sampling rate of 1000 Hz was used for all experiments presented here. Fig. 3(b) shows the averaged STE obtained by running the experimental set-up in the same configuration as was used to obtain Fig. 3(a).

This averaging technique follows the same principles as the well known signal processing technique of dither [21]. Prior to sampling, the dynamical signal is comprised the repeatable STE function and additional noise, which we assume is random. When this signal is digitised by the encoder, the quantised values at a particular phase of the STE will oscillate between the digital levels above and below the actual value of the STE at that phase, due to the additional noise. If the assumption of random noise is correct, then the average of the quantised data points will tend to the actual signal as number of samples tends to infinity.

By taking the fast Fourier transform of the STE and extracting the amplitudes and phases of the largest power spectrum components, it is possible to recreate a STE with less noise. As the gross rotation rate for these tests was 1 Hz, the frequencies shown are normalised to the gross rotation rate (i.e. a component of the STE at 2 Hz describes the amplitude of

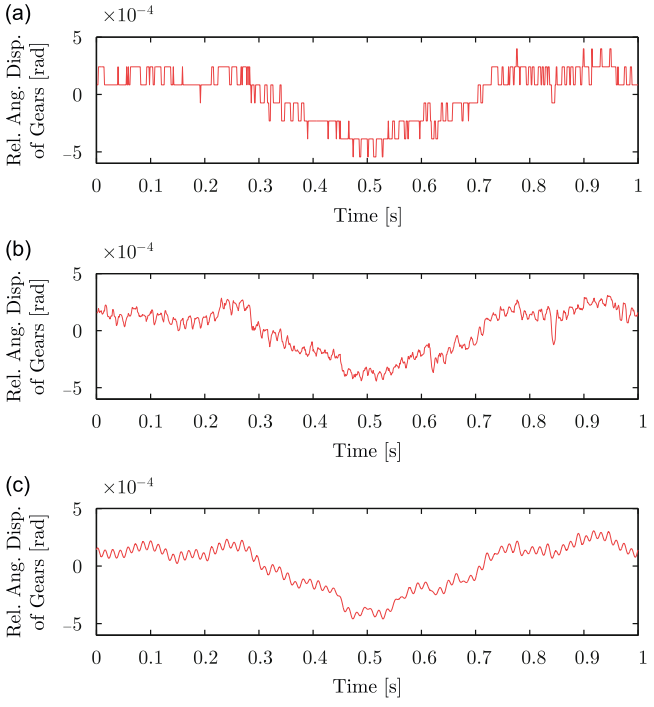

Fig. 3. Generating an error function from experimental data. (a) The STE signal obtained from the encoders over one rotation. (b) An STE generated by averaging each data point over 25 rotations. (c) The error function generated using a 'selective filtering' technique.

errors that occur twice every rotation, 3 Hz occur three times every rotation etc.). We express our STE function as

$$e(\tau)=\sum_{j\in f}a_j\cos(j\theta_1+\phi_j), \tag{11}$$

where f is the set of frequencies considered and a_j and ϕ_j relate to the amplitude and phase of the cosine at the specified frequency. Here, the amplitudes and phases of the largest 21 power spectrum amplitudes are used. These frequencies generally relate to the meshing frequency (18 teeth on each gear rotating at 1 Hz causing a meshing frequency of 18 Hz), tooth errors (eccentricity at 1 Hz, random, 'phantom' errors [22,23] at various other frequencies) and combinations and harmonics of each. It was not within the scope of this work to derive expressions for the error that each of these frequencies corresponds to, although the first-order terms that are due to eccentricity, have been calculated in previous work (see Eq. (7) in Ref. [14], $a_1 = U$ and $\phi_1 = d$).

The STE function of the rig in one configuration is given in Fig. 3(c). The generated STE is very similar to the recorded transmission errors. The advantage of this method is that we have a smooth continuous depiction of the STE which may be differentiated to obtain the velocity and acceleration due to STE at any time. This is necessary if we wish to substitute this STE function into our mathematical model for analytical purposes.

4.1. Damping due to meshing losses

As each tooth pair meshes, the mating tooth surfaces rub (and roll) against each other. Combined with fluid film effects due to gear lubricants, the interaction of the gears would appear to become much more complicated, with losses incurred at each tooth contact. Modelling friction between gear teeth is not a trivial task due to the load and velocity dependence of friction forces [15,16,18] as well as the nonlinearity induced by the instantaneous change in direction of friction forces as a tooth pair rotates past the pitch point [16–19].

Being unlubricated and running at low speed, the findings of this earlier research [16–19] would suggest that friction may have an affect on gear rattle. Continuing with the basic modelling approach, we consider the absorbing energy of the friction force as a linear damping coefficient. When the gears are in contact we effectively have a higher non-dimensional damping coefficient which we denote δ_{contact}. Therefore, Eq. (9) becomes

$$x''=2\pi\delta_{\text{contact}}-2\pi\varepsilon\sqrt{4\pi^2+\delta_{\text{contact}}^2}\cos\left(2\pi\tau+\phi-\arctan\left(\frac{\delta_{\text{contact}}}{2\pi}\right)\right)-e''(\tau)-\delta_{\text{contact}}e'(\tau),\quad |x|=\beta, \tag{12}$$

$$x''+\delta x'=2\pi\delta-2\pi\varepsilon\sqrt{4\pi^2+\delta^2}\cos\left(2\pi\tau+\phi-\arctan\left(\frac{\delta}{2\pi}\right)\right)-e''(\tau)-\delta e'(\tau),\quad x<\beta, \tag{13}$$

where the gears are treated as in contact in the first equation when $|x|=\beta$ and out of contact in the second equation.

In order to establish a value for δ_{contact} we conduct run-down tests on the experimental rig. The technique involves driving the gear pair up to speed then removing any external forcing acting on the system. Angular displacement readings, recorded using the encoders, of the subsequent run-down motion were then used to ascertain experimental damping values.

As no external forcing acts on the driven shaft during run-down, and assuming that the motion may be adequately described by linear inertial and damping coefficients, the equation of motion for the drive shaft is

$$I\ddot{\theta}_2+c\dot{\theta}_2=0. \tag{14}$$

By setting the initial displacement to zero, $\theta_2(0)=0$, and by requiring that the displacement as time tends to infinity is given by $\theta_2(t\to\infty)=\theta_\infty$, the solution to Eq. (14) may be given as

$$\theta_2=\theta_\infty(1-\mathrm{e}^{-(c/I)t}). \tag{15}$$

We may rearrange Eq. (15) to give

$$-\frac{c}{I}t=-\delta\Omega t=\ln(\theta_\infty-\theta_2)-\ln(\theta_\infty), \tag{16}$$

where δ is the dimensionless damping defined in Eq. (8).

Initially the gear pair was unmeshed, and run-down tests on both the drive side and the driven side of the rig in isolation were conducted. These tests established how the linear viscous friction of each shaft varies with angular speed. Then a run-down test was conducted for the meshed gear pair. If there are no losses at the mesh interface, the damping value generated from run-down test for the meshed gear pair would have been equal to the sum of the dampings generated by the run-down test conducted for the two unmeshed gears. However, additional losses at the mesh interface cause the damping value of the run-down test for the meshing case to be in excess of the sum of the damping values of the two unmeshed gears.

The results of the run-down tests are shown in Fig. 4(a). Fig. 4(b) shows the damping curve due to friction, generated by subtracting the damping values of the two sides of the rig from the damping value of the entire rig. We observe that the value of damping is velocity dependent. This is because at lower speeds, the components of dry coulomb friction in the

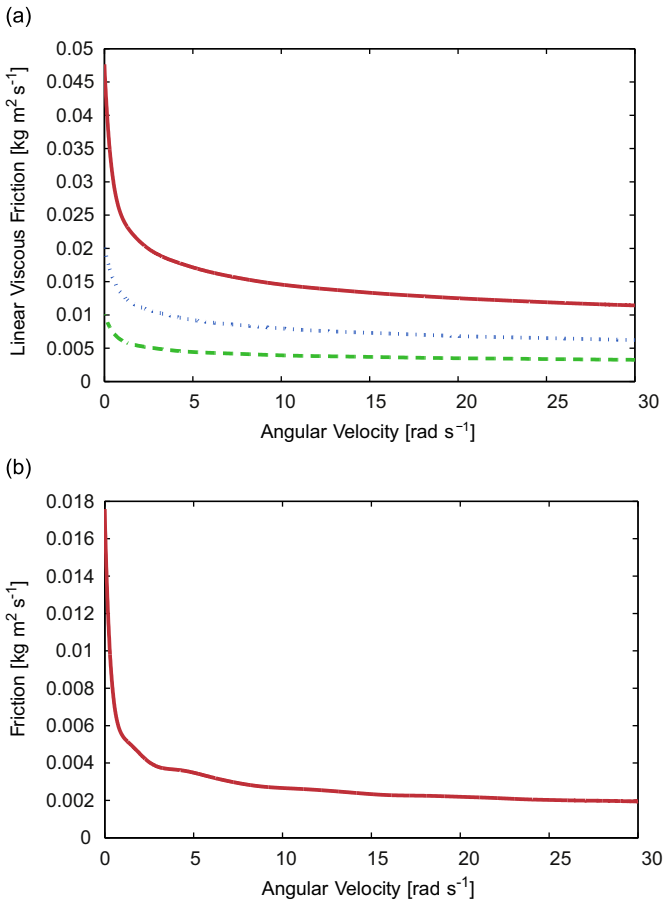

Fig. 4. Results of the run-down tests used to obtain a value describing losses at the mesh interface. (a) Instantaneous linear viscous damping coefficient as a function of angular velocity for each test. Solid line: meshed gear pair; dashed line: drive gear (unmeshed) and dot-dash line: driven gear (unmeshed). (b) How damping due to losses at the mesh interface varies with angular velocity. This curve was generated by subtracting the sum of the damping values for the unmeshed drive and driven gears from the damping value for the meshed gear pair.

bearings increase in magnitude. Therefore the total damping forces increase and the shaft decreases its speed at a faster rate it slows.

5. Comparisons between experimental and theoretical results

For the purpose of comparing the mathematical model with experimental findings, the error function was generated using the findings from the experimental rig. By linking the experimental recordings to results of the mathematical model using this method of generating the error function, it is possible prove the link between internal meshing errors, whatever they may be, to rattle response.

We begin by developing time domain trajectories which we can compare with the experimental data recorded from the encoders. Initially we assume that the gears are meshing together, so that Eq. (12) is the relevant equation of motion. We note that once the right-hand side of Eq. (12) (i.e. the relative forcing between the gears) becomes negative the relative acceleration must also become negative and the gears must lose contact. When this occurs Eq. (13) becomes valid. The solution of Eq. (13), truncated so as to only include values in the range $-\beta < x < \beta$, with initial conditions defined by the change in sign of the relative forcing, represents the free-play motion that occurs due to this contact loss.

Due to the servomotor having a low moment of inertia (which allows for accurate control of forcing amplitudes and phases), the coefficient of restitution observed experimentally is extremely low. In this instance we make the assumption that the gears immediately re-mesh once they impact. This is effectively equivalent to a coefficient of restitution of zero, $\varsigma = 0$. This increases the ease with which we may incorporate friction into the model; once the point at which the gears re-mesh has been established we may again begin the process of checking whether the right-hand side of Eq. (12) is less than zero (with the new starting point in time when the gears re-meshed from the previous contact loss).

Fig. 5 shows comparisons between experimental and theoretical results, considering the STE function given in Fig. 3. We consider three different phases of external displacement sinusoidal input for the case where the external displacement

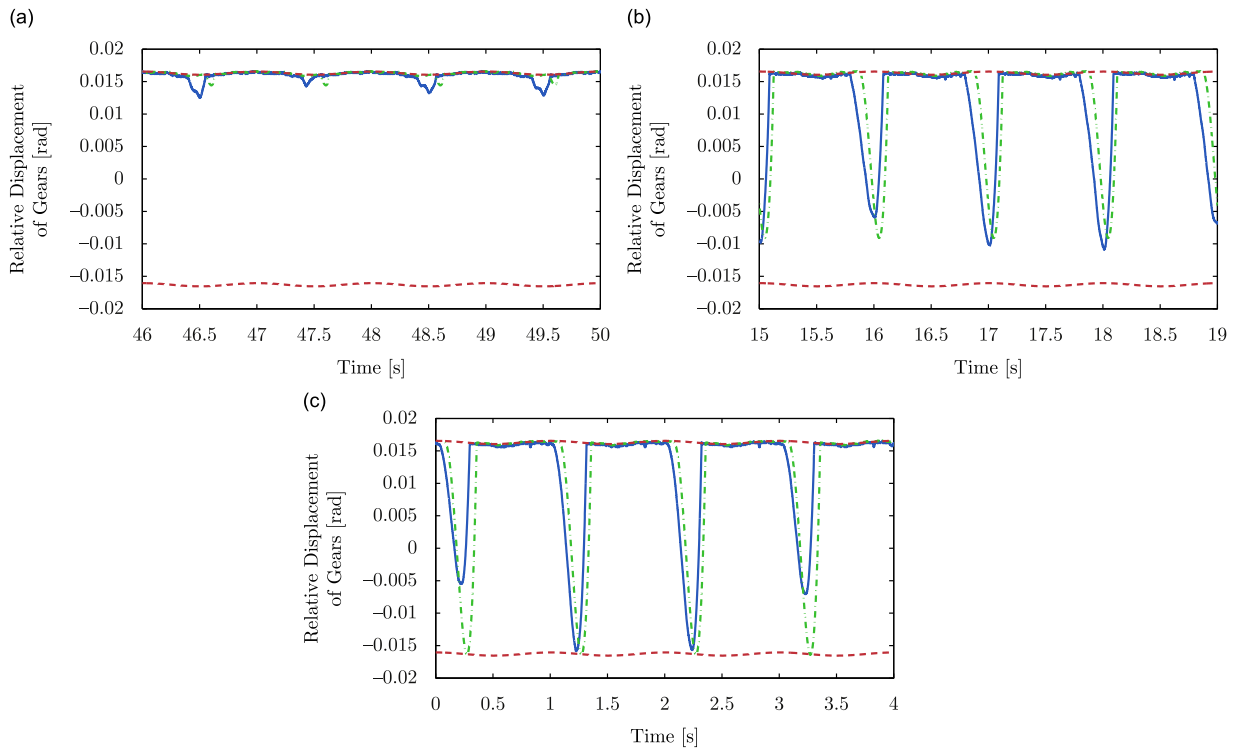

Fig. 5. Comparisons of trajectories obtained experimentally with those generated theoretically for non-dimensional parameter values $\delta = 2.3$, $\delta_{\text{contact}} = 4.2$, $\beta = 1.63 \times 10^{-2}$, $\varepsilon = 0.43$. Solid line: experimental data; dashed line: backlash boundaries; dot-dash line: theoretical trajectory. (a) Small amplitude rattle comparison, phase of forcing relative to phase of eccentricity = 2.60 rad. (b) Medium amplitude rattle comparison, phase of forcing relative to phase of eccentricity = 5.14 rad. (c) Large amplitude rattle comparison, phase of forcing relative to phase of eccentricity = 0.25 rad.

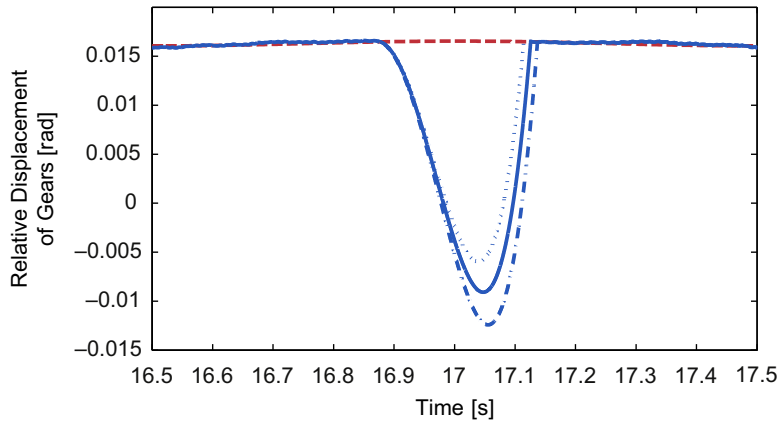

Fig. 6. The effect of changing the phase of forcing by a small amount in the mathematical model. Solid line: reference trajectory (phase of forcing relative to phase of eccentricity = 5.14 rad); dashed line: positive drive backlash boundary; dot-dash line: theoretical trajectory where the input forcing lags the reference by 0.035 rad; dotted line: theoretical trajectory where the input forcing leads by 0.035 rad. Non-dimensional parameter values: $\delta = 2.3$, $\delta_{\text{contact}} = 4.2$, $\beta = 1.63 \times 10^{-2}$, $\varepsilon = 0.43$.

fluctuation amplitude is 0.43 rad. In order to compare with the experimental findings of [14] we relate the phase of the external displacement input to the phase of the order one components of the STE, which are primarily due to eccentricities. The non-dimensional damping, δ, is taken from run-down tests to be 2.3. Note that as the forcing due to the STE can theoretically allow for contact loss at any time, we use a damping value measured at the gross rotation rate of the system. The non-dimensional damping whilst in contact, δ_{contact}, was measured to be 4.2 and the half backlash, β, was 1.63×10^{-2}. In each figure the solid line is experimental data and the dot-dash line is the equivalent trajectories generated from the mathematical model. The dashed lines represent the backlash boundaries. We observe strong agreement between the

experimental and theoretical findings. Clearly, the effect of changing the phase of the input and hence the magnitude of the relative forcing between the gears is to change the amplitude of rattle response.

It has previously been reported that the amplitude of each disconnection is highly variable [14]. One possible cause of this is sensitivity to parameters such as impact time and amplitude. Using the model, Fig. 6 shows the effect of a small variation in phase on the theoretical response on the system. The solid line indicates the theoretical response previously shown in Fig. 5(b), the reference in this instance. The dashed line shows the response with a phase of external displacement fluctuation changed so as to lead the reference by 0.035 rad (2°), whilst the dot-dash line shows the response with the phase of external displacement fluctuation lagging the reference by 0.035 rad (2°). The selection of 0.035 rad is arbitrary, simply necessary to illustrate the effect of a small change to the phase of the input. We see that this small change in the phase of the input results in a large change in the amplitude of the response. This change in the phase of the input is equivalent to a small change in the amplitude of the relative forcing at the interface. Therefore, small variations to the relative forcing at the interface caused by system noise may result in noticeable variations in the amplitude of the response, as we have observed experimentally.

In order to investigate the effectiveness of this mathematical model over a range of forcing amplitudes and phases contour plots similar to those presented in [14] may be produced. We accomplish this by again assuming that initially the gears are meshing on the $x=\beta$ surface. By finding the point at which the right-hand side of Eq. (12) becomes negative and then solving Eq. (13) we may obtain trajectories for a range of amplitudes, ε and phases, ϕ of input forcing. In this instance we have considered input amplitudes between $\varepsilon=0.39$ and 0.46 in increments of 0.005 as well as 50 different input phases between $\phi=0$ and 2π. We then plot the maximum displacement away from the positive drive $x=\beta$ boundary of each trajectory against input phase and amplitude. We reference our input phase as being relative to the phase of the order one component of the static transmission error, which is primarily due to eccentricity.

As discussed in Section 3, for 1:1 ratio gear pairs, a change in the initial alignment of the driven gear relative to the drive gear, Ψ, will result in a change in the STE function. Due to alignment tolerances between the gear and shaft centres the maximum amplitude of the STE can vary considerably. We are therefore able to create different STE functions simply by

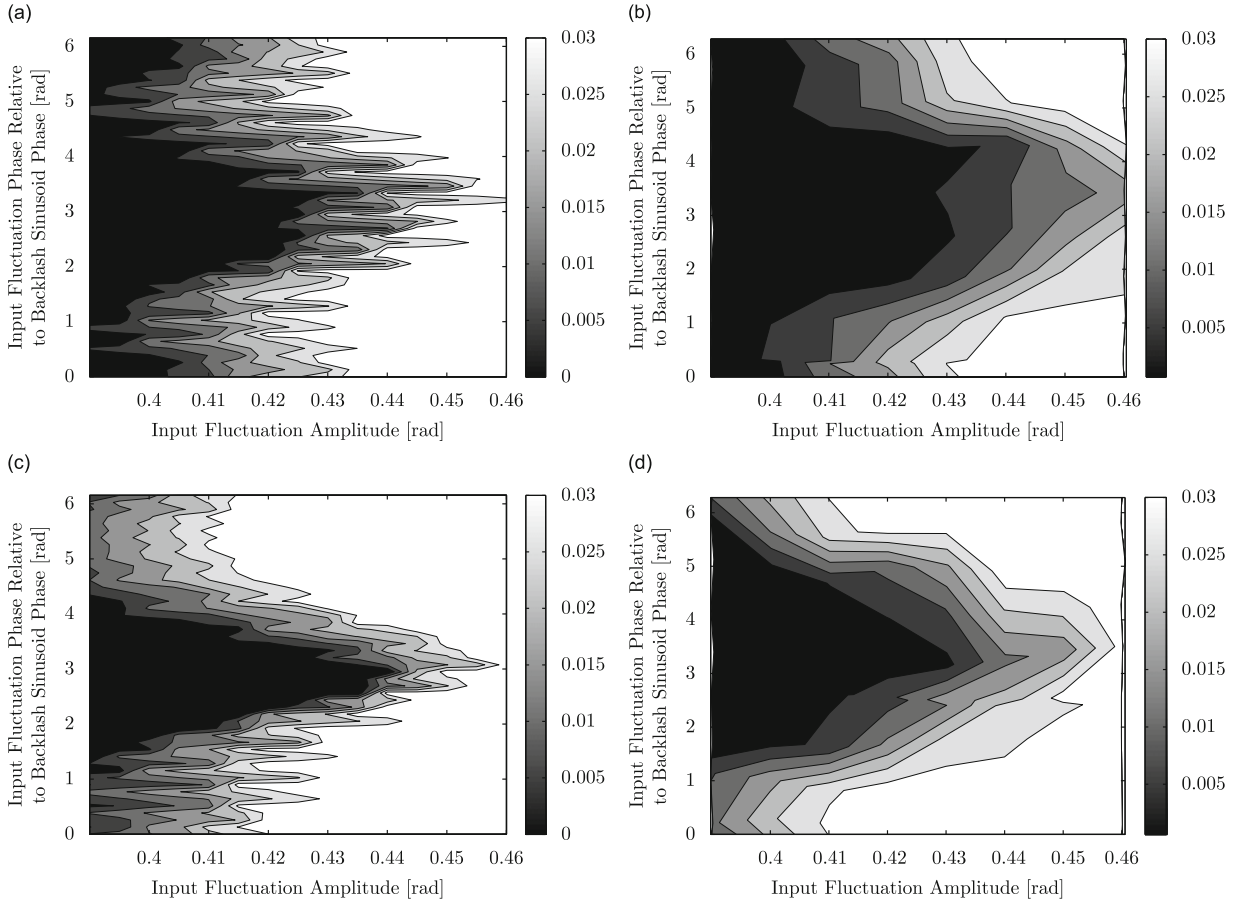

Fig. 7. Comparison of contour plots generated both theoretically with those generated experimentally for three different experimental static transmission cases. Non-dimensional parameter values: $\delta=2.3$, $\delta_{\text{contact}}=4.2$, $\beta=1.63\times10^{-2}$, $\varepsilon=0.39$–0.46. (a) and (c) Theoretical contour plots for eccentricity cases (i) and (ii), respectively and (b), (d) corresponding experimental data for the two eccentricity cases.

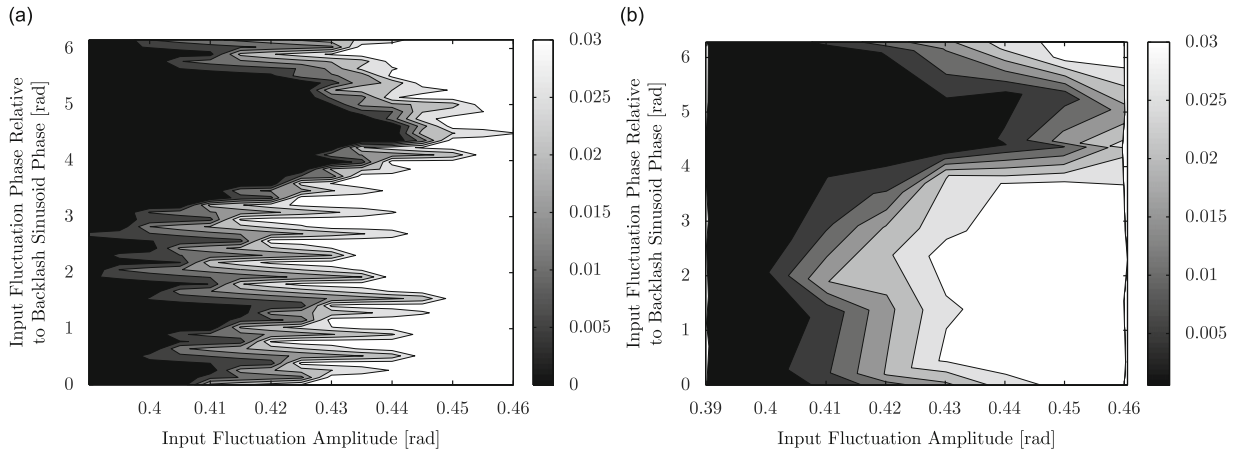

Fig. 8. Comparison of contour plots generated both theoretically with those generated experimentally for three different experimental static transmission cases. Non-dimensional parameter values: $\delta = 2.3$, $\delta_{\text{contact}} = 3.7$, $\beta = 1.63 \times 10^{-2}$, $\varepsilon = 0.39{-}0.46$. (a) Theoretical contour plot for case (iii) and (b) corresponding experimental data.

changing which tooth pairs mesh with one another. Four STE profiles will be considered, three with low maximum amplitudes; case (i) 0.3×10^{-3} rad case (ii) 2.5×10^{-4} rad and case (iii) 2×10^{-4} rad and one with a higher maximum amplitude; case (iv) 9.5×10^{-3} rad. Note that cases (i) and (iv) correspond to cases B and C in [14], whilst case (iii) corresponds to case A when running the rig in reverse (see Section 12 in [14]). Fig. 7 shows the theoretical contour plots for two different experimental static transmission error cases. The figures on the left-hand side are the theoretical contour plot and next to them on the right-hand side of the figure are the equivalent experimental curves (Fig. 7(b) has previously been given in [14]).

Fig. 8 shows the theoretical contour plots for case (iii) (Fig. 8(b) has previously been given in [14]). In order to generate this plot it has been necessary to fit a value for the in-contact damping value with theoretical results. It was found that a value of $\delta_{\text{contact}} = 3.7$ gave good agreement. It is believed that this lower value of in-contact damping was due to the alignment of the eccentricities. In this case, the eccentricities were aligned so as to give the smallest possible component of static transmission error at the gross rotation rate (i.e. due to eccentricities). As a result there was less relative motion between gear teeth and hence we may surmise that frictional losses are less.

The model-based contour plots have largely the same shapes as those based on experimental data. Changing the STE function changes the shape of the theoretical contour plots, broadly to match the equivalent experimental curves. The theoretical plots appear to be much more complex than the experimental ones. It is thought that this is due to the averaging technique used when determining the amplitude of disconnection for each experiment, to remove the small variations in response to noise driven parameter variations. Our theoretical model does not model this random feature, so captures just one of the tooth disconnection trajectories. This emphasises the point that the variability in amplitude of response observed in some experiments may be described by small perturbations in system parameters; the theoretical curves show the exact amplitude of response for a given phase and amplitude of forcing, but diverge from that given phase and amplitude by a small amount so that the amplitude of response may change drastically.

Fig. 9 shows a case where the method we have employed seemingly breaks down. The figure shows the theoretical contour plots for the alignment which creates the largest STE due to eccentricity, case (iv). Fig. 9(a) is the theoretical contour plot and Fig. 9(b) (previously given in Ref. [14]) is the equivalent experimental contour plot. Whilst showing qualitative agreement in amplitude and general shape of the contours, the contour appears to have been shifted by approximately π radians. This may possibly be explained by the basic method we have employed for modelling friction.

The friction constant δ_{contact} is based on the assumption that the same frictional losses occur throughout the complete meshing sequence of the two gears. However, the manufacturing errors which comprise the STE will cause the reaction forcing between the gears to vary, as the imposed change in displacement caused by a meshing error is resisted by the inertial forces of the free gear. This in turn changes the instantaneous friction coefficient. This variation will be small providing the STE is small. However, in the larger eccentricity case (case (iv)) the alignment of the eccentricities is such that the reaction forcing between the gears may vary enough to cause the assumption of constant friction to only be accurate in a qualitative sense.

The model used to generate these results assumed a damping coefficient which was not a function of speed whereas the experimental rundown tests clearly suggest otherwise. This assumption simplified the modelling and analysis of the system. Fig. 10 shows a theoretical contour plot for case (i) generated using a numerical time-stepping model with the experimentally measured frequency-dependent damping coefficient. The damping value at each velocity value is obtained by interpolating the experimentally obtained damping values given in Fig. 4. It can be seen that there is very little

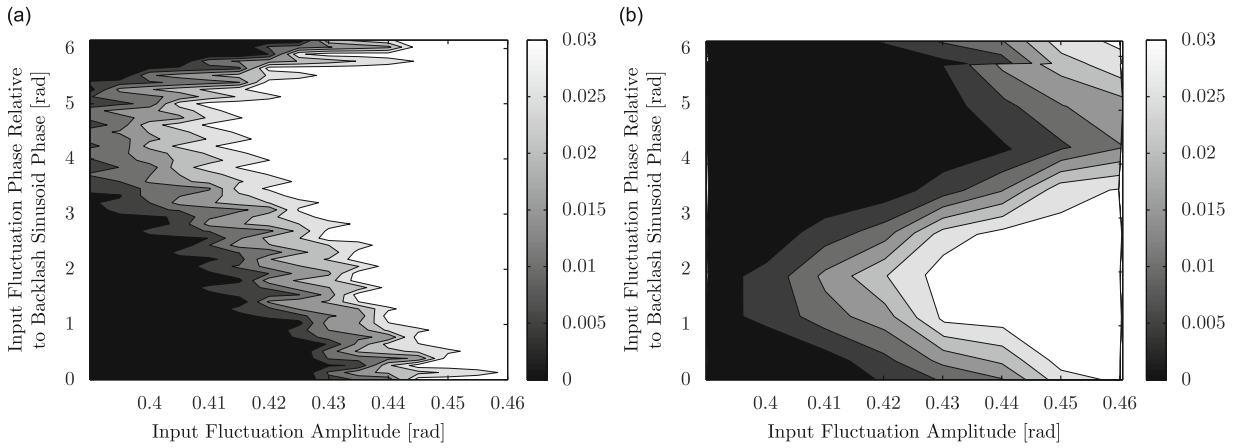

Fig. 9. Comparison of contour plots generated both theoretically with those generated experimentally for a large magnitude experimental static transmission error. (a) Theoretical contour plot for the large amplitude STE case (iv) (Case C from Ref. [14]). non-dimensional parameter values: $\delta = 2.3$, $\delta_{\text{contact}} = 4.2$, $\beta = 1.63 \times 10^{-2}$, $\varepsilon = 0.39{-}0.46$. (b) Equivalent experimental data to (a).

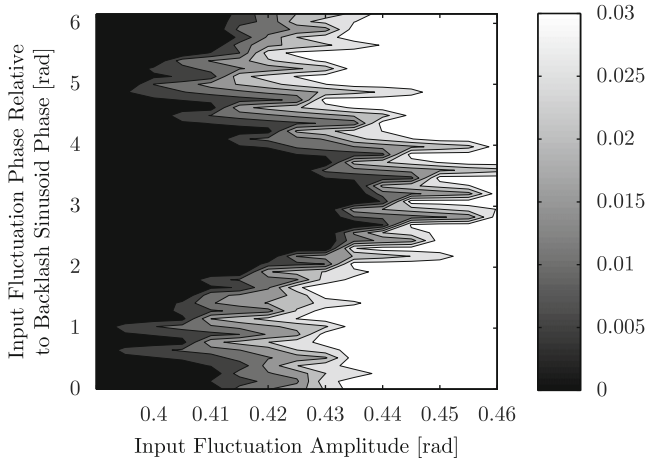

Fig. 10. Contour plot created using an angular velocity dependent damping for eccentricity cases (i). This contour plot may be compared with the equivalent contour plot calculated using a linear damping coefficient (Fig. 7(a)). Non-dimensional parameter values: $\beta = 1.63 \times 10^{-2}$, $\varepsilon = 0.39{-}0.46$. Both in-mesh and freeplay damping values are found by interpolating the damping curves given in Fig. 4.

difference between Fig. 10 and the equivalent contour plot for a linear damping model (Fig. 7(a)), thus justifying the assumption made for these experiments.

6. Conclusions

The ground gears used in these experiments are extremely accurate. The tooth errors that remain produce a small STE with a maximum size of 0.95×10^{-3} rad or an arc length of 51 μm at the pitch circle radius. Despite this, in this paper we have shown that such tiny tooth errors can have a major effect on gear rattle. Firstly, we considered gear rattle caused by the relative forcing between the gears overcoming the damping forces, as was investigated experimentally in [14]. We began by developing a method for synthesising a STE function from experimental data. We then derived an equation of motion into which this error function may be substituted. We also introduced an 'in contact' damping parameter, which incorporated the losses that occur at the mesh interface due to friction, which was justified by a series of run-down tests. We were then able to solve the equations of motion to generate trajectories and contour plots which agreed well with experimental results. We observed:

- Changing the phase of an external forcing input changes the relative forcing between the gears, and so changes the amplitude of gear rattle.

- Other small perturbations, that are an inevitable feature of real systems, can have a large effect on gear rattle amplitude. This explains the seemingly random amplitude responses observed in some experiments.
- Once the magnitude of the STE grows too large the model breaks down. We hypothesise that a more complex friction analysis is required to describe the motions of grossly inaccurately manufactured gears.

We conclude that the total STE must be incorporated when considering gear rattle due to forcing fluctuations at the interface exceeding the damping forces. This is because the STE of even highly accurate gear pairs (as were used in this case) contributes so heavily to those interface forcing fluctuations. This explains the perceived unpredictability of gear rattle and intermittent behaviour. The complexity of the STE, the phase and amplitude of the forcing input (which in practice will generally be unpredictable) and inherent system noise cause the forcing transmitted through the interface and hence, the size of any contact losses to vary vastly. We have shown that in the majority of cases (provided the assumption of constant friction coefficient holds), gear rattle may be predicted by the superposition of the error forcing and the external forcing.

The simple lumped model proposed here achieves very good agreement with experimental findings when the eccentricity is not dominated by misalignment between gear and shaft centres. Using this modelling approach it is clear which areas require further investigation. This paper highlights the importance of future investigation into accurate friction and damping models as well as improvements in modelling the STE.

Acknowledgements

J.R.O. gratefully acknowledges the support of a CASE award from Jaguar Cars and the Engineering and Physical Sciences Research Council.

References

[1] R. Singh, H. Xie, R.J. Comparin, Analysis of automotive neutral gear rattle, *Journal of Sound and Vibration* 131 (2) (1989) 177–196.
[2] F. Pfeiffer, A. Kunert, Rattling models from deterministic to stochastic processes, *Nonlinear Dynamics* 1 (1990) 63–74.
[3] W.D. Mark, Contributions to the vibratory excitation of gear systems from periodic undulations on tooth running surfaces, *Journal of the Acoustical Society of America* 91 (1992) 166–186.
[4] W.A. Tuplin, *Gear Design*, first ed., The Machinery Publishing Co. Ltd., London, UK, 1962.
[5] H.N. Özgüven, D.R. Houser, Mathematical models used in gear dynamics, *Journal of Sound and Vibration* 121 (1988) 383–411.
[6] S.L. Harris, Dynamic loads on the teeth of spur gears, *Proceedings of the Institution of Mechanical Engineers* 172 (1958) 87–99.
[7] R.W. Gregory, S.L. Harris, R.G. Munro, Dynamic behaviour of spur gears, *Proceedings of the Institution of Mechanical Engineers* 178 (1963) 207–217.
[8] A. Kahraman, R. Singh, Non-Linear dynamics of a spur gear pair, *Journal of Sound and Vibration* 142 (1) (1990) 49–75.
[9] S. Theodossiades, S. Natsiavas, Periodic and chaotic dynamics of motor-driven gear-pair systems with backlash, *Chaos, Solitons and Fractals* 12 (2001) 2427–2440.
[10] H.N. Özgüven, D.R. Houser, Dynamic analysis of high speed gears by using loaded static transmission error, *Journal of Sound and Vibration* 125 (1) (1988) 71–83.
[11] W.D. Mark, Use of the generalized transmission error in the equations of motion of gear systems, *Journal of Mechanisms Transmissions and Automation In Design—Transactions of the ASME* 109 (2) (1987) 283–291.
[12] S. Theodossiades, O. Tangasawi, H. Rahnejat, Gear teeth impacts in hydrodynamic conjunctions promoting idle gear rattle, *Journal of Sound and Vibration* 303 (3–5) (2007) 632–658.
[13] C.K. Halse, R.E. Wilson, M. di Bernardo, M.E. Homer, Coexisting solutions and bifurcations in mechanical oscillators with backlash, *Journal of Sound and Vibration* 305 (2007) 854–885.
[14] J.R. Ottewill, S.A. Neild, R.E. Wilson, Intermittent gear rattle due to interactions between forcing and manufacturing errors, *Journal of Sound and Vibration* 321 (2009) 913–935.
[15] H. Iida, A. Tamura, Y. Yamada, Vibrational characteristics of friction between gear teeth, *Bulletin of JSME* 28 (241) (1985) 1512–1519.
[16] P. Velex, V. Cahouet, Experimental and numerical investigations on the influence of tooth friction in spur and helical gear dynamics, *Journal of Mechanical Design* 122 (4) (2000) 515–522.
[17] M. Vaishya, R. Singh, Strategies for modeling friction in gear dynamics, *Journal of Mechanical Design* 125 (2) (2003) 383–393.
[18] M. Vaishya, R. Singh, Sliding friction-induced non-linearity and parametric effects in gear dynamics, *Journal of Sound and Vibration* 248 (4) (2001) 671–694.
[19] M. Vaishya, R. Singh, Analysis of periodically varying gear mesh systems with Coulomb friction using Floquet theory, *Journal of Sound and Vibration* 243 (3) (2001) 525–545.
[20] J. Mason, M. Homer, R.E. Wilson, Mathematical models of gear rattle in roots blower vacuum pumps, *Journal of the Sound and Vibration* 308 (2007) 431–440.
[21] S.W. Smith, *The Scientist and Engineer's Guide to Digital Signal Processing*, second ed., California Technical Publishing, San Diego, CA, USA, 1997.
[22] W.D. Mark, Analysis of the vibratory excitation of gear systems: basic theory, *Journal of the Acoustical Society of America* 63 (5) (1978) 1409–1430.
[23] J.D. Smith, *Gear Noise and Vibration*, first ed., Marcel Dekker Inc., New York, NY, USA, 1999.